Available online at www.sciencedirect.com
ScienceDirect
Journal of Geochemical Exploration 91 (2006) 81–98
JOURNAL OF GEOCHEMICAL EXPLORATION
www.elsevier.com/locate/jgeoexp

Geochemical patterns of schists from the Bushmanland Group: An artificial neural networks approach

J.P. Lacassie [a,b,*], C.R. McClung [a], R.H. Bailie [a], J. Gutzmer [a], J. Ruiz-Del-Solar [c]

[a] *Paleoproterozoic Mineralization Research Group, Department of Geology, University of Johannesburg, Auckland Park, Johannesburg, 2006, Republic of South Africa*
[b] *Servicio Nacional de Geología y Minería, Avda. Santa María 0104, Casilla 10465, Santiago, Chile*
[c] *Departamento de Ingeniería Eléctrica, Universidad de Chile, Casilla 412-3, 6513027 Santiago, Chile*

Received 7 January 2005; accepted 17 March 2006
Available online 13 July 2006

Abstract

The Mesoproterozoic Bushmanland Group is situated in the central region of the 1000 to 1200 Ma Namaqualand Metamorphic Complex (NMC). The NMC comprises a belt of highly deformed medium- to high-grade metamorphic rocks to the west of the Archean Kaapvaal Craton of southern Africa. The Bushmanland Group, one of the many supracrustal sequences that make up the NMC, is a metavolcano-sedimentary succession that hosts economically significant concentrations of sillimanite and base-metal sulfide deposits. The present investigation was carried out to study the geochemistry of a large set of representative samples of psammo-pelitic schists from the Bushmanland Group, which includes data from three different schist units: Namies Schist Formation, Shaft Schist Formation and Ore Equivalent Schist. The objective was three-fold: to test the lateral correlatability of these schist units as determined by field relationships, to identify the geochemical signature of the schists and to test the validity of an Artificial Neural Network approach as an exploration tool. Two multidimensional datasets, respectively comprising 10 major and 18 trace elements, were constructed using selected published schist analyses. Both schist datasets were analyzed using self-organizing neural maps for visualizing and clustering high-dimensional geochemical data. Geochemical differences between the various schists were visualized using colored two-dimensional maps that can be visually and quantitatively interpreted. The results of this study confirm the lateral correlatability of the schist units evaluated in this communication. It was also found that each schist unit or portions of them represent a distinct geochemical signature that is related to true lithological variations. The results show that the Artificial Neural Network approach can be used as a powerful tool for regional mineral exploration in poly-deformed and metamorphosed terrains where identification of stratigraphic units through lateral correlation by means of fieldwork and petrography remains highly speculative.

Keywords: Neural networks; Visual analysis; Geochemical exploration; Base-metal mineralization; South Africa

1. Introduction

Defining common groups or clusters, as referred to in data analysis and pattern recognition, and relating them to geologic constraints or processes at local, regional or global scales are fundamental tasks of any geochemical evaluation. However, large geochemical datasets often impede recognition of complex patterns of correlation between variables, association among samples and anomaly identification. Conventional parametric multivariate statistical procedures may be obscured by the presence of multivariate outliers, non-normal variable distributions and non-linear correlations among variables

* Corresponding author. Tel.: +56 2 7375050.
E-mail address: jlacassi@ing.uchile.cl (J.P. Lacassie).

0375-6742/$ - see front matter © 2006 Elsevier B.V. All rights reserved.
doi:10.1016/j.gexplo.2006.03.004

in the high-dimensional spaces under analysis. On the contrary, self-organizing neural maps, a special group of unsupervised trained Artificial Neural Networks (ANN), provides a non-linear, rapid and robust tool for analyzing geochemical multivariate data. By using self-organizing maps for clustering and for the non-linear projection of high-dimensional data onto lower dimensional displays (visualization), relevant geochemical information can be exhibited in a maximally concentrated form. Moreover, outlying observations can be included in the dataset without significantly affecting the main patterns and relationships identified.

In this study, we use the Growing Cell Structures (GCS) self-organizing maps (Fritzke, 1994) for finding visual representations of multi-dimensional geochemical data of schists from the Mesoproterozoic Bushmanland Group of the Northern Cape Province, South Africa. Two large geochemical datasets have been projected onto two-dimensional representations where the most relevant information for the clustering task is discovered through simple, visual inspection.

The Bushmanland Group represents a supracrustal succession of the Namaqualand Metamorphic Complex and is renowned for hosting economically significant deposits of gypsum, halite, bismuth, pegmatitic minerals, sillimanite, base-metal sulfides, barite and dimension stone (Wilson and Anhaeusser, 1998). Centered on the towns of Aggeneys and Pella (Fig. 1), the Bushmanland Group hosts approximately 400 Mt of 6 wt.% Pb+Zn+Cu, 19.1 g/t Ag, 6 Mt of barite ore (Novak and Kihn, 1994; Du Toit, 1998; Stalder and Rozendaal, 2005; Black Mountain Mine, unpublished data) and roughly 1 Mt of sillimanite ore (De Jager and von Backström, 1961; De Jager, 1963). Although continued exploration for these deposits in this highly prospective terrain remains a high priority, the poly-deformed and metamorphosed nature of the host rock succession continues to hamper both the identification of prospective units and stratigraphic correlation both locally and regionally.

In this contribution and as part of a larger study evaluating the lithostratigraphy of the Bushmanland Group, an ANN approach for finding visual representations of high-dimensional geochemical data for the schists of the Bushmanland Group where two large geochemical datasets have been projected onto two-dimensional representations where the most relevant

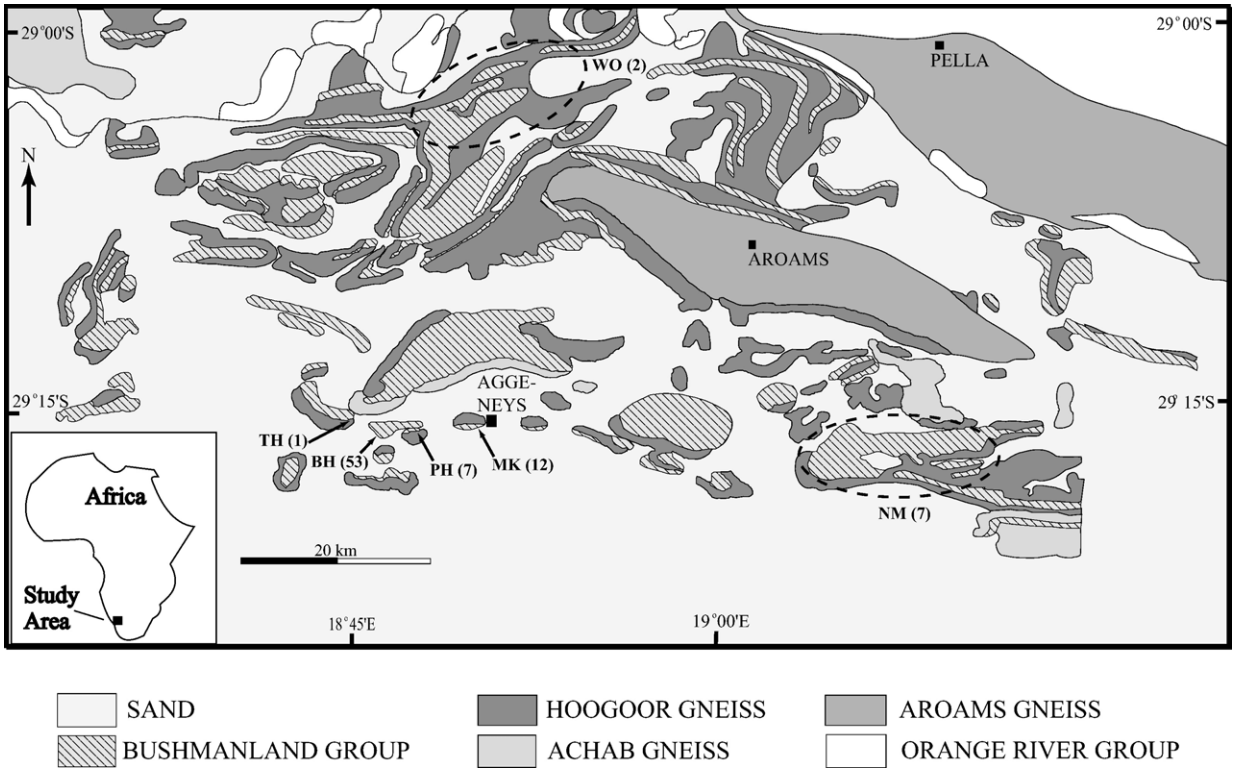

Fig. 1. Geographical distribution of the samples used in this study. The number of selected samples is indicated in parentheses at the right of the respective locality acronym: Broken Hill (BH); Tank Hill (TH); Plant Hill (PH); Maanhaarkop (MK); Namiesberg (NM); Wortel (WO) (modified after Reid et al., 1997).

information for the clustering task is discovered through simple visual inspection. This has been used to aid in these regional correlations, in the identification of geochemical signatures and as a tool for exploration.

2. Geological setting

The moderately to highly metamorphosed and poly-deformed metavolcano-sedimentary rocks of the

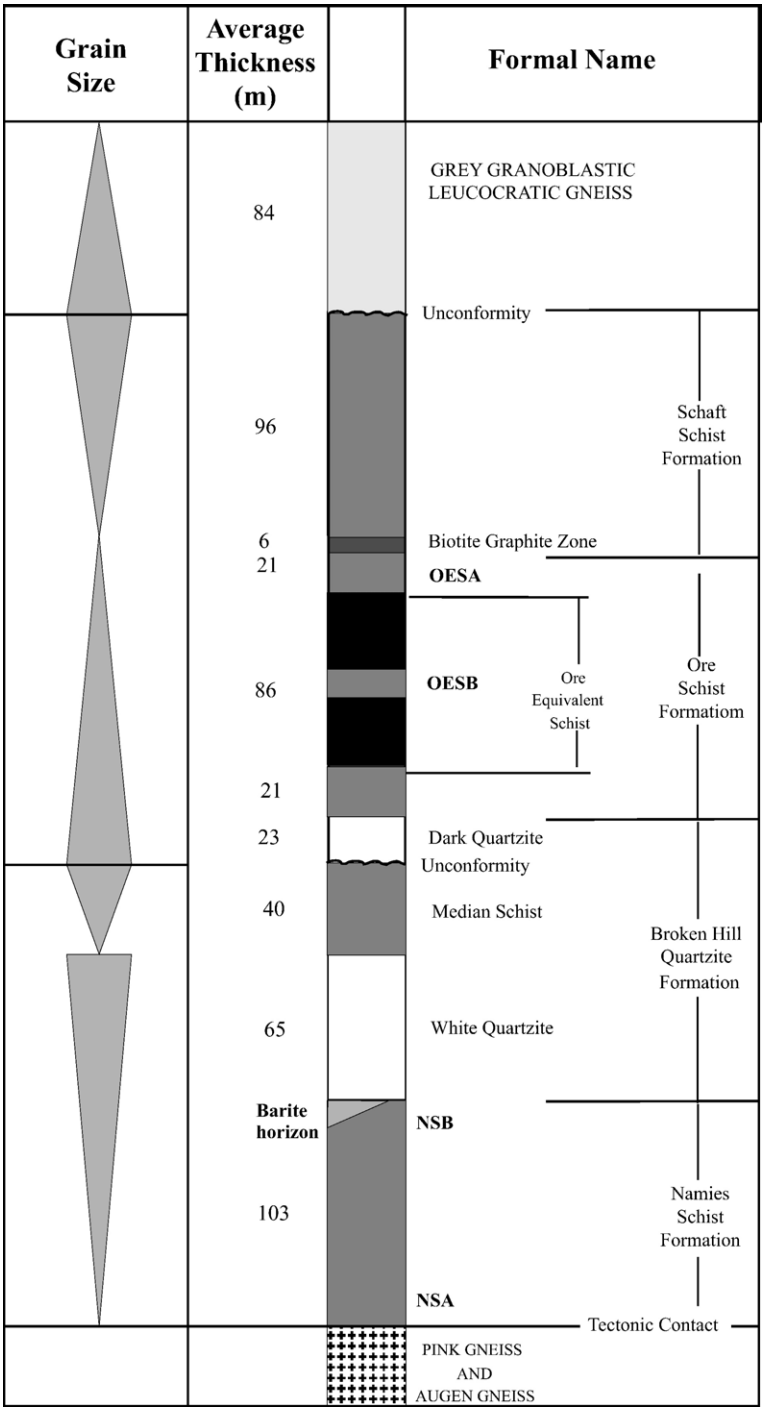

Fig. 2. Generalized stratigraphic column of the Bushmanland Group (stratigraphic subdivision of Lipson, 1990). The vertical grain size variation is indicated by the graphical scale on the left. Modified after Lipson (1990) and McClung (in preparation).

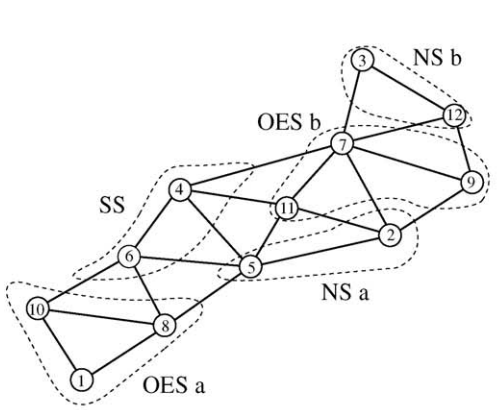
NS b
OES b
SS
NS a
OES a
1
2
3
4
5
6
7
8
9
10
11
12

(a)

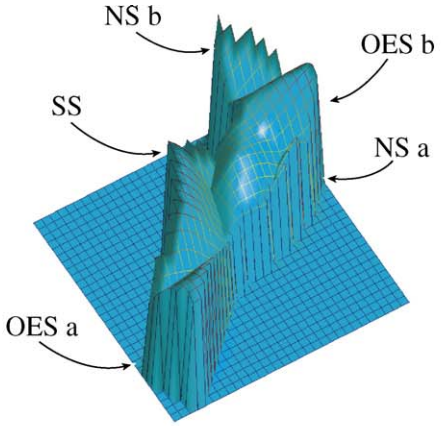
NS b
OES b
SS
NS a
OES a

(b)

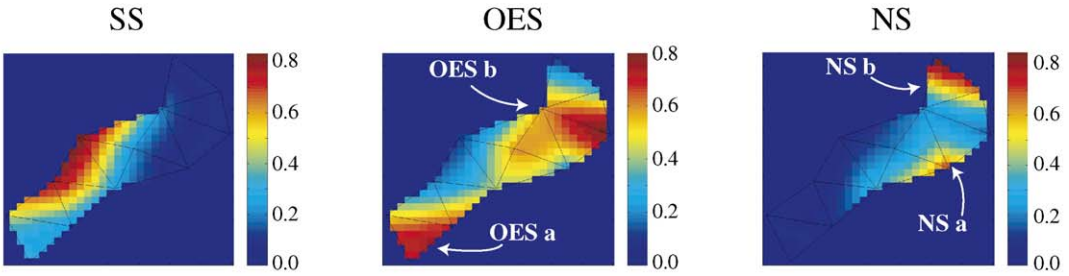
SS
OES
NS
OES b
OES a
NS b
NS a
0.8
0.6
0.4
0.2
0.0

(c)

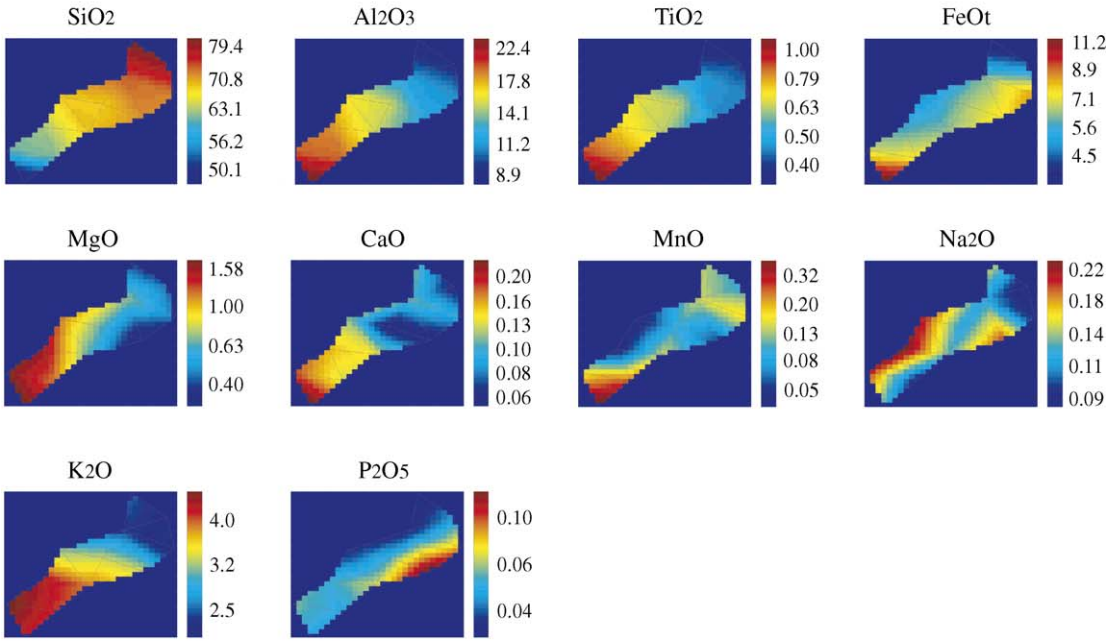
SiO2
79.4
70.8
63.1
56.2
50.1
Al2O3
22.4
17.8
14.1
11.2
8.9
TiO2
1.00
0.79
0.63
0.50
0.40
FeOt
11.2
8.9
7.1
5.6
4.5
MgO
1.58
1.00
0.63
0.40
CaO
0.20
0.16
0.13
0.10
0.08
0.06
MnO
0.32
0.20
0.13
0.08
0.05
Na2O
0.22
0.18
0.14
0.11
0.09
K2O
4.0
3.2
2.5
P2O5
0.10
0.06
0.04

(d)

Bushmanland Group form the western extension of the Namaqualand Metamorphic Complex (NMC; Joubert, 1974) and represent the remains of an ancient mobile belt. In the Aggeneys–Gamsberg District (Fig. 1), the Bushmanland Group constitutes a roughly 1000 m thick succession of mineralogically mature quartzites and psammo-pelitic schists with minor intercalations of mafic metavolcanic rocks. Using the stratigraphic subdivision of Lipson (1990), the Bushmanland Group consists of a basal pelitic to psammitic schist (Namies Schist Formation), a mixed quartzite and schist unit (Broken Hill Quartzite Formation) conformably overlain by pelitic schists (Ore Schist and Shaft Schist Formations). The entire sequence is unconformably capped by a package of psammitic schist, conglomerates and ortho-amphibolites of the Koeris Formation (Fig. 2).

The Namies Schist Formation (NS) is one of the economically most important units, as it hosts all of the sillimanite deposits, the largest being the Swartkoppies deposit near Pella (Fig. 1). Comprised of an approximately 75 to 100 m thick sequence of highly foliated, brown (weathered) to grey-green (fresh) psammo-pelitic schists, the NS is conformably overlain by the orthoquartzites of the Broken Hill Quartzite Formation. The Broken Hill Quartzite Formation constitutes a 155 m thick unit that is subdivided into a basal White Quartzite, intermediate Median Schist and upper Dark Quartzite. The basal White Quartzite is a massive, grey to milky-white, medium- to coarse-grained orthoquartzite. The Median Schist conformably overlies the White Quartzite where it occurs as an irregular, discontinuous horizon between the two quartzite layers, displaying a similar texture and character to the NS. The Dark Quartzite unconformably overlies the Median Schist (C.R. McClung, unpublished data) and has a similar mineralogy as the White Quartzite. The Ore Schist Formation gradationally overlies the Dark Quartzite. The Ore Schist Formation, the second economically significant unit, hosts all of the sulfide and barite deposits of the Aggeneys–Gamsberg District (Fig. 1). In general, the Ore Schist Formation varies in thickness from 100 to 200 m thick (Ryan et al., 1986; Lipson, 1990) and consists of a succession of interbedded pelitic schists, similar in composition to those of the lower NS, and dark, micaceous quartzites. At the Broken Hill deposit (Fig. 1), the Ore Schist Formation has been further subdivided, from oldest to youngest, into: Hangingwall Schist, Upper Ore Body, Intermediate Schist, Lower Ore Body, and Upper Footwall Schist. The ore bodies, in combination with the Intermediate Schist, grade laterally into the Ore Equivalent Schist (OES). The top of the Ore Schist Formation is marked by the presence of a thin, approximately 6 m thick zone characterized by a highly foliated, black, graphitic schist. This unit marks the stratigraphic top of the Ore Schist Formation. The Shaft Schist Formation (SS) conformably overlies the Ore Schist Formation and comprises an approximately 100 m thick sequence of pelitic schist with a similar texture and composition to the other schists of the Bushmanland Group. The Koeris Formation, a roughly 300 m thick unit of psammitic schists, metaconglomerate and ortho-amphibolites, unconformably caps the Shaft Schist Formation (Fig. 2).

While the NMC has been subjected to five deformational and metamorphic events (Joubert, 1986; Ryan et al., 1986; Lipson, 1990; Hoffmann, 1993), only the last four of these have been positively identified in the Aggeneys area (Ryan et al., 1986; C.R. McClung, unpublished data). The second and most intense deformational event is characterized by amphibolite to granulite facies metamorphism (650 to 690 °C, 3.5 to 4.5 kbar; Ryan et al., 1986; Lipson, 1990) with synchronous isoclinal folding and subsequent thrusting (Colliston and Schoch, 2002; C.R. McClung, unpublished data). The third phase of deformation consists of retrograde metamorphism and large-scale open and monoclinal folding, in addition to the development of numerous faults, fractures and shear zones.

3. Petrography

3.1. Namies Schist Formation

The Namies Schist Formation is composed of quartz, biotite, fibrolitic sillimanite, garnet (spessartine–almandine), muscovite, microcline, cordierite, pyrite, chalcopyrite, sphalerite and magnetite, with sillimanite and biotite locally forming large concentrations of up to 40% of the rock (Moore, 1989). Common accessory minerals include plagioclase, staurolite, tourmaline, rutile,

Fig. 3. Visualization of posterior probabilities and input variable distributions for a 12-node GCS map trained on 79 cases for the log-normalized major element dataset (Table 2; Appendix A). (a) Stratigraphic-related unit distribution over the GCS map structure. All the nodes are numbered and labeled: Shaft Schist Formation (SS); Ore Equivalent Schist (OES); Namies Schist Formation (NS). (b, c) Three-dimensional (b) and two-dimensional (c) visualization of the posterior probability distributions. Five clusters have been modeled by the network, with clear separation between each. One is associated with the Shaft Schist Formation (SS), two are associated with the Ore Equivalent Schist (OESa and OESb), whereas the other two are associated with the Namies Schist Formation (NSa and NSb). For the two-dimensional visualization (c) the posterior probability concentrations are shown by the color axes at right. (d) Two-dimensional visualization of the distributions of the input variables. Distributions of each variable can easily be compared visually with that of the posterior probabilities, and with each other. The scales at right indicate whole rock concentrations (wt.% oxide).

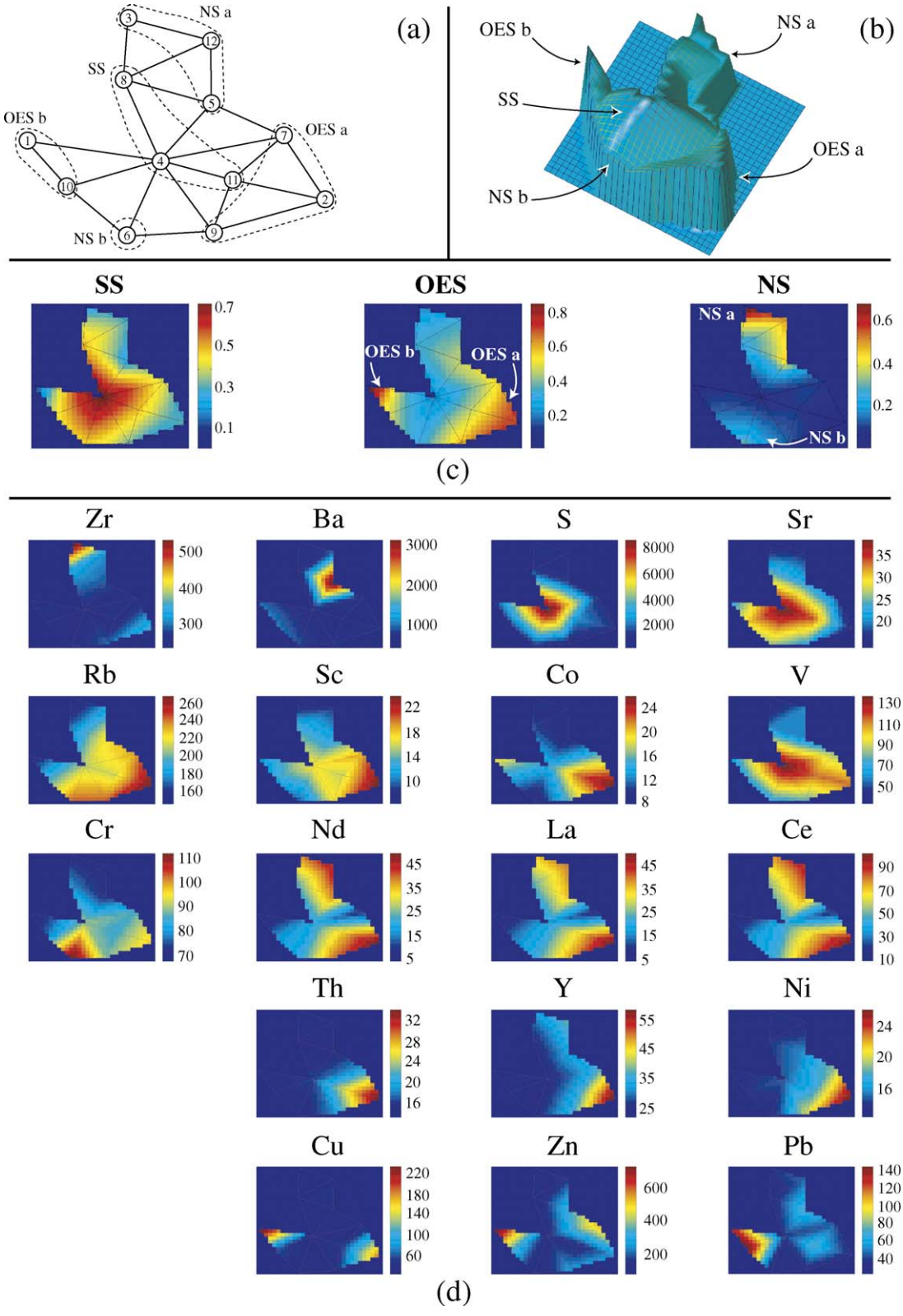
(a)
NS a
SS
OES b
OES a
NS b
1
2
3
4
5
6
7
8
9
10
11
12
(b)
OES b
NS a
SS
OES a
NS b
(c)
SS
0.7
0.5
0.3
0.1
OES
OES b
OES a
0.8
0.6
0.4
0.2
NS
NS a
NS b
0.6
0.4
0.2
(d)
Zr
500
400
300
Ba
3000
2000
1000
S
8000
6000
4000
2000
Sr
35
30
25
20
Rb
260
240
220
200
180
160
Sc
22
18
14
10
Co
24
20
16
12
8
V
130
110
90
70
50
Cr
110
100
90
80
70
Nd
45
35
25
15
5
La
45
35
25
15
5
Ce
90
70
50
30
10
Th
32
28
24
20
16
Y
55
45
35
25
Ni
24
20
16
Cu
220
180
140
100
60
Zn
600
400
200
Pb
140
120
100
80
60
40

anatase, apatite, hematite, ilmenite, zircon and monazite (Ryan et al., 1986). The feldspars have been extensively sericitised and the biotite has been chloritised to varying degrees.

3.2. Ore equivalent Schist

The Ore Equivalent Schist consists of biotite, garnet and quartz with lesser amounts of muscovite. Accessory amounts of zircon, gahnite, magnetite, apatite and sphene have also been identified.

3.3. Shaft Schist Formation

The Shaft Schist Formation is characterized by quartz, sillimanite, biotite, muscovite, pyrite and graphite with an accessory amount of zircon. Muscovite and biotite have been extensively sericitised. Compared to the Namies Schist Formation, the Shaft Schist Formation contains a lower concentration of garnet, cordierite, staurolite and zircon, but higher concentrations of sillimanite, biotite and muscovite.

4. Methodology

The geochemical dataset of Lipson (1990) was used to examine geochemical patterns in the metapelitic schists of the Bushmanland Group. These include data from three different stratigraphic units as defined by Lipson (1990) and earlier workers, namely: (1) the Namies Schist (NS) and (2) Shaft Schist (SS) Formations, and (3) the Ore Equivalent Schist (OES) of the Ore Schist Formation. Two datasets were constructed using selected sample analyses. These were: (1) *Log-normalized major element dataset*: comprising log-normalized values for 79 schist samples with concentration data (wt.%) for the ten major and minor oxides (SiO_2, TiO_2, Al_2O_3, K_2O, Na_2O, CaO, FeOt, MgO, MnO and P_2O_5), and (2) *Trace element dataset:* comprising 81 samples with concentrations (ppm) for 18 trace elements (Ba, Ce, Co, Cr, Cu, La, Nd, Ni, Pb, Rb, S, Sc, Sr, Th, V, Y, Zn and Zr) in all samples. Both datasets include samples of each stratigraphic unit, collected from six different localities: Broken Hill, Plant Hill, Tank Hill, Maanhaarkop, Namiesberg and Wortel. For both datasets the selection criteria was based on a trade-off between the number of samples and the number of elements per sample. The samples are not evenly distributed between stratigraphic units and localities (Fig. 1). In the log-normalized major element dataset, 44% of the samples are from the SS, 40% from the OES, and 16% from the NS (Appendix A). In the trace element dataset 48% are from the SS, 32% from the OES, and 20% from the NS (Appendix B).

Table 1
Stratigraphic related cluster distribution of the analyzed datasets

Cluster	% NS	% OES	% SS
Log-normalized major element dataset			
NS	97	0	0
OES	3	86	0
SS	0	14	100
Total	100	100	100
Trace element dataset			
NS	86	4	8
OES	7	86	2
SS	7	10	90
Total	100	100	100

Note: For each dataset, the percentage values (%) refers to the percentage of training samples of each stratigraphic unit that was assigned to each stratigraphic-related cluster, as defined by their respective nodes or map units (Figs. 3 and 4). The percentage values (%) were calculated from Appendices A and B. SS: Shaft Schist Formation; OES: Ore Equivalent Schist; NS: Namies Schist Formation.

Each one of these high-dimensional datasets (10 and 18 dimensions, respectively) were projected by the GCS algorithm onto two-dimensional representations or feature maps, where the most relevant information for the clustering task is easily discovered through visual inspection. For each stratigraphic unit, the GCS algorithm converts the frequency of data samples assigned to each node or map unit (prior probability) into a prediction for a new sample associated to each node (posterior probability; Fritzke, 1994). The posterior probabilities of the different stratigraphic units are then displayed on color maps, which overlay the final map structure (e.g. Fig. 3C). Alternatively, for generating a three-dimensional visualization, the posterior probabilities can be displayed as altitudes, i.e. *Z*-axis values, ranging between 0 and 1 (e.g. Fig. 3B).

Fig. 4. Visualization of posterior probabilities and input variable distributions for a 12-node GCS map trained on 81 cases for the trace element dataset (Table 4; Appendix B). (a) Stratigraphic-related unit distribution over the GCS map structure. All the nodes are numbered and labeled: Shaft Schist Formation (SS); Ore Equivalent Schist (OES); Namies Schist Formation (NS). (b, c) Three-dimensional (b) and two-dimensional (c) visualization of the posterior probability distributions. Five clusters have been modeled by the network, with clear separation between four of them. One is associated with a specific stratigraphic unit, the Shaft Schist Formation (SS), two are associated with the Namies Schist Formation (NSa and NSb), whereas the other two are associated with the Ore Equivalent Schist (OESa and OESb). For the two-dimensional visualization (c) the posterior probability values are shown by the color axes at right. (d) Two-dimensional visualization of the distributions of the input variables. Distributions of each variable can easily be compared visually with that of the posterior probabilities, and with each other. The scales at right indicate whole rock concentrations (ppm).

Table 2
Average concentrations of the major elements in each of the five identified stratigraphic-related units of the Bushmanland Group (Fig. 3)

	NSa	NSb	OESa	OESb	SS	PAAS
SiO_2	70.7	82.7	59.5	70.7	65.7	62.8
Al_2O_3	13.6	8.4	20.1	13.2	17.7	18.9
TiO_2	0.57	0.37	0.92	0.57	0.71	1.0
FeO_T	7.00	3.93	8.31	7.21	5.25	5.67
MnO	0.12	0.13	0.35	0.21	0.04	0.11
MgO	0.50	0.41	1.41	0.65	1.48	2.2
CaO	0.12	0.10	0.20	0.09	0.13	1.3
K_2O	3.65	2.39	4.29	2.73	3.75	3.7
Na_2O	0.17	0.12	0.16	0.11	0.25	1.2
P_2O_5	0.10	0.04	0.05	0.10	0.04	0.16

The concentrations of the Post-Archean Average Australian Shale (PAAS) (McLennan, 1989) are shown for reference. All data in wt.%.

Average values for individual input variables at each node can also be displayed on color maps and overlain on the final map structure allowing simple visual comparison with the posterior probability color maps (e.g. Fig. 3D). Those input variables whose color map distributions are similar to the posterior probability color map distribution of a particular stratigraphic unit are highly likely to be significant discriminating elements for that stratigraphic unit (e.g. S correlating with the SS on the color map distributions in Fig. 4). Similarly, if two or more input variables have similar color map distributions (e.g. Al_2O_3 and TiO_2 color map distributions in Fig. 3), a close correlation exists between them. For both datasets no *a priori* knowledge was used during the unsupervised training of the GCS neural map or in determining its structure (both the map structure and the node weights are automatically adapted from the input data). The class information tagged to each analysis was used only after the GCS training algorithm determined the final map structure. Therefore, the final structure appears in the trained network as a natural characteristic of the samples of the two analyzed datasets. For a more detailed explanation of the methodology the reader is referred to Lacassie et al. (2004).

5. Results

The ANN analyses of the NS, OES and SS resulted in two distinct network topologies or maps for the major and trace elements respectively (Figs. 3 and 4). The numerical results of Table 1 show that, for the log-normalized major element dataset, the NS and SS define the best clusters (i.e. the highest percentages of correctly assigned samples). The OES has a less well-defined clustering (i.e. lower percentages of correctly assigned samples) due mainly to the relatively large dispersion of this cluster towards the SS. Compared to the log-normalized major element dataset, cluster definition in the trace element dataset decreases for the NS and SS clusters (Table 1). Particularly relevant is the NS dispersion towards the OES, whereas poorer definition of the SS cluster is due to increased dispersion of the SS towards the NS. Both GCS maps (Figs. 3 and 4) allow visualization of the role of each input variable (major and trace elements) in the overall separation of the stratigraphic-related clusters.

5.1. Log-normalized major element dataset

The GCS algorithm modeled the major element dataset as five different stratigraphic-related clusters or units (Fig. 3). One is associated with the SS, two with the OES (OESa and OESb), and two with the NS (NSa and NSb). Visual inspection of the GCS map (Fig. 3) allows recognition of a strong correlation between Al_2O_3 and TiO_2, a good correlation between FeOt and MnO, and, to a lesser extent, between MgO and CaO.

The major element results are summarized in Table 2 and are compared to the average value of Post Archean Australian Shale (PAAS) (McLennan, 1989). Relative to PAAS all the units are depleted in TiO_2, MgO and P_2O_5, strongly depleted in CaO and Na_2O, and, except OESa, enriched in SiO_2 and depleted in Al_2O_3. Apart from SS all the units are enriched in MnO relative to PAAS.

In terms of major element concentrations (wt.%), the GCS map shows clear contrasts and affinities among the five units (Fig. 3; Tables 2 and 3; Appendix A). Relatively high to very high P_2O_5 abundances are typical of NSa. Low TiO_2, Al_2O_3, FeOt and MgO coupled with high SiO_2 concentrations are characteristic of NSb. Low Na_2O concentrations are associated with NSb and OESb. OESa is characterized by a broad range of intermediate to low concentrations of SiO_2 and relatively high concentrations of Al_2O_3, TiO_2, FeOt, MnO, CaO and K_2O. SS is characterized by low MnO and high Na_2O values.

5.2. Trace element dataset

The GCS network modeled the trace element data as four distinct clusters or units, as well as a poorly defined fifth with the division reflecting that of the major element suite (Fig. 4). Visual inspection of the GCS map (Fig. 4) allows recognition of a good correlation between Zn and Pb, a good correlation between Nd, La and Ce, a good to moderate correlation between Th, Ni and Y, and a moderate correlation between Sc and Rb.

The trace element results are summarized in Table 4 and compared to concentrations in Post Archean Australian Shale (PAAS) (McLennan, 1989). Relative to PAAS all the units are depleted in Sr, Ni, Co and V,

enriched in Rb, Zr and Nd, and, except NSb, enriched in Zn and Pb. NSa and OESa are enriched in Y, whereas the other units are depleted in that element. Only NSa is enriched in La and Ce relative to PAAS, while only OESa and OESb are enriched in Cu relative to PAAS. OESa and SS are enriched in Th and Sc, whereas all the other units are depleted in those elements. In contrast, only OESa and SS are depleted in Ba relative to PAAS. Apart from NSb all units are depleted in Cr.

In terms of trace element concentrations (ppm), the GCS map shows clear contrasts and affinities among the five units (Fig. 4; Tables 4 and 5; Appendix B). NSa is characterized by relatively high La and Ba concentrations. Relatively high Cr and low La, Ce, Nd, Zn, Pb and S are typical of NSb. Both NS units (NSa and NSb) are also characterized by relatively low abundances of Co and Sc. High Rb, Y, Th, Ni and Sc concentrations are typical of OESa. Both OES units (OESa and OESb) are also characterized by relatively high Co concentrations. Very high Pb, Zn and Cu concentrations are restricted to OESb, which is also characterized by relatively low Rb concentrations. Very high abundances of S are typical of

Table 3
Average and standard deviation elemental concentrations in each stratigraphic-related node, for the GCS map resulting from the analysis of the log-normalized major element dataset (Fig. 3)

Stratigraphic-related nodes	SiO_2	Al_2O_3	FeOt	MnO	MgO	CaO	Na_2O	K_2O	TiO_2	P_2O_5
Major and minor oxides										
SS nodes										
4 avg.	69.20	16.21	4.80	0.04	1.22	0.12	0.24	3.08	0.68	0.03
4 std.	1.89	1.03	0.42	0.02	0.20	0.03	0.07	0.32	0.04	0.01
6 avg.	62.41	19.01	5.67	0.04	1.72	0.15	0.26	4.39	0.74	0.05
6 std.	1.66	0.54	0.65	0.01	0.12	0.04	0.07	0.36	0.04	0.01
SS avg.	65.69	17.66	5.25	0.04	1.48	0.13	0.25	3.75	0.71	0.04
SS std.	3.87	1.63	0.70	0.02	0.30	0.04	0.07	0.75	0.05	0.02
OESa nodes										
1 avg.	40.30	26.56	18.26	0.88	1.79	0.51	0.15	3.79	1.35	0.04
1 std.	6.02	2.96	2.44	0.01	0.66	0.23	0.02	0.54	0.45	0.01
8 avg.	62.43	19.13	7.29	0.34	1.05	0.13	0.08	4.08	0.81	0.05
8 std.	2.74	1.41	1.09	0.08	0.22	0.02	0.02	0.88	0.05	0.02
10 avg.	61.53	19.39	6.51	0.20	1.83	0.20	0.27	4.78	0.95	0.06
10 std.	2.01	1.84	1.13	0.14	0.16	0.05	0.08	0.47	0.27	0.01
OESa avg.	59.51	20.09	8.31	0.35	1.41	0.20	0.16	4.29	0.92	0.05
OESa std.	7.73	2.92	3.94	0.23	0.47	0.14	0.10	0.79	0.26	0.02
OESb nodes										
7 avg.	74.32	10.84	6.67	0.37	0.92	0.14	0.11	2.19	0.46	0.03
7 std.	0.88	0.25	0.29	0.39	0.25	0.04	0.05	0.33	0.01	0.01
9 avg.	72.22	11.22	8.52	0.23	0.53	0.13	0.09	2.12	0.48	0.10
9 std.	1.58	1.29	1.36	0.12	0.30	0.13	0.02	0.37	0.10	0.04
11 avg.	68.60	15.26	6.42	0.15	0.67	0.05	0.12	3.31	0.66	0.05
11 std.	1.96	1.42	0.82	0.17	0.26	0.02	0.05	0.79	0.10	0.02
OESb avg.	70.71	13.18	7.21	0.21	0.65	0.09	0.11	2.73	0.57	0.07
OESb std.	2.80	2.47	1.39	0.19	0.28	0.08	0.04	0.84	0.13	0.04
NSa nodes										
2 avg.	72.43	11.15	7.91	0.06	0.26	0.08	0.23	3.25	0.44	0.16
2 std.	2.53	1.77	2.00	0.05	0.11	0.05	0.06	0.39	0.19	0.01
5 avg.	69.64	14.98	6.46	0.16	0.65	0.14	0.14	3.89	0.65	0.07
5 std.	1.57	1.10	0.98	0.05	0.19	0.03	0.05	0.53	0.09	0.02
NSa avg.	70.68	13.55	7.00	0.12	0.50	0.12	0.17	3.65	0.57	0.10
NSa std.	2.31	2.35	1.50	0.07	0.25	0.05	0.07	0.56	0.16	0.05
NSb nodes										
3 avg.	83.76	7.93	3.52	0.22	0.36	0.17	0.20	2.55	0.32	0.03
3 std.	1.32	1.03	1.22	0.08	0.06	0.01	0.08	0.10	0.15	0.01
12 avg.	81.95	8.77	4.20	0.07	0.45	0.05	0.08	2.29	0.41	0.04
12 std.	1.71	0.51	1.51	0.04	0.08	0.03	0.01	0.21	0.06	0.02
NSb avg.	82.67	8.43	3.93	0.13	0.41	0.10	0.12	2.39	0.37	0.04
NSb std.	1.52	0.70	1.15	0.08	0.07	0.06	0.07	0.19	0.09	0.01

Abbreviations: SS: Shaft Schist Formation; OES: Ore Equivalent Schist; NS: Namies Schist Formation. Note: Averages and standard deviations have been calculated using the values of Appendix A. "Misclassified" samples are not included in these calculations.

Table 4
Average concentrations of the trace elements in each of the five identified stratigraphic-related units of the Bushmanland Group (Fig. 4)

	NSa	NSb	OESa	OESb	SS	PAAS
Rb	176	252	263	163	201	160
Ba	1363	900	500	911	453	650
Sr	15	23	19	22	33	200
Zr	429	243	267	238	268	210
La	39	22	36	25	27	38
Ce	87	41	79	52	59	80
Nd	43	20	38	25	27	19
Y	37	23	40	22	24	27
Th	15	12	23	14	17	15
Ni	14	11	22	14	15	55
Co	8	6	19	18	15	23
Sc	8	8	21	12	17	16
V	42	53	89	57	119	150
Cr	67	179	105	66	98	110
Cu	33	30	55	198	33	50
Zn	233	59	396	666	124	85
Pb	63	14	40	170	47	20
S	281	91	222	133	6403	No data

The concentrations within the Post-Archean Average Australian Shale (PAAS) (McLennan, 1989) are shown for reference. All data in ppm.

SS as well as relatively high Sr, intermediate Sc and relatively low Ba concentrations.

6. Discussion

6.1. Comparison between GCS and Discriminant Function Analysis

Discriminant Function Analysis (DFA) is a multivariable statistical technique that is commonly used to visualize first-order differences between groups of samples. In DFA the groups or clusters are determined beforehand and the object is to determine the linear combination of independent variables which best discriminates among the groups. This is done by creating a new variable from the independent variables such that it provides the maximum linear separation between group centers. This process repeats with successive new variables that further separate the group centers. Therefore DFA is a ''supervised'' technique that will not distinguish ''natural'' groups within sets of data, as it relies upon prior knowledge of the groupings (Le Maitre, 1982). A DFA is also sensitive to outliers, assumes multivariate normality and that the variability within groups is similar for the independent variables and, being a type of linear fitting, rejects non-linear relations between samples or variables. In contrast, in GCS analysis the groups or clusters are not predetermined and the higher-order correlations between the variables are also taken into account.

In DFA the relative importance of the discriminating variables can be assessed by comparing the standardized discriminant coefficient ratios. In contrast, GCS maps allow visual perception of the relationships between variables. Therefore, in GCS analysis the relevant factors responsible for the cluster structures and the meaningful correlations between relevant discriminating factors can be visually identified.

Self-organized maps have been successfully tested with geochemical analyses of such different materials as stream sediments (Lacassie et al., 2003a), sandstones (Lacassie et al., 2004), manganese nodules (Achurra et al., 2003) and zircon grains (Lacassie et al., 2003b). Those studies have shown that GCS visualization has clear interpretative and analytical advantages over other commonly used linear-based numerical approaches. In particular, Lacassie et al. (2003b) have shown that GCS analysis has considerable potential for unveiling additional relevant information not seen by other linear-based multivariate statistical procedures, by comparing the final results of GCS maps and of principal component analysis (PCA). The reason for this is that GCS is a non-linear analysis tool, and therefore does not have the limitations of linear-analysis methods, dissimilar to DFA and PCA.

6.2. Cluster definition

As *a priori* knowledge was not used during the unsupervised training of the GCS map, the clustering or group separation appears in the trained network as a natural characteristic of the samples of the two datasets analyzed. The cluster dispersions among stratigraphic-related clusters (Table 1) are probably a reflection of the geochemical similarities between the different stratigraphic units. However, they are also related to the proportion of "misclassified" data that is associated with each cluster of the GCS maps (Appendices A and B).

The psammo-pelitic schist units of the Aggeneys–Gamsberg District (Fig. 1) have been characterized by stratigraphic and petrographic analyses, as well as application of statistical techniques on the geochemistry of these units. According to Lipson (1990), on simple petrographic grounds the schists at Broken Hill and Maanhaarkop (Fig. 1) can be correlated with a high degree of certainty, although the correlations with the schists at Tank Hill appears more tenuous. On the farm Wortel, 8 km to the north of Aggeneys, a comparable stratigraphic sequence occurs (Lipson, 1990). For both databases, the great majority of the samples from Plant Hill, Tank Hill, Maanhaarkop and Wortel (Fig. 1) have been correlated by the GCS map with a high degree of

Table 5
Average and standard deviation elemental concentrations in each stratigraphic-related nodes, for the GCS map resulting from the analysis of the trace element dataset (Fig. 4)

Stratigraphic-related nodes	Pb	Zn	Cu	Ba	Co	Cr	Ni	Rb	S	Sc	Sr	Th	V	Y	Zr	La	Ce	Nd
Trace elements																		
SS nodes																		
4 avg.	44	147	40	514	15	107	15	218	10573	19	38	17	158	23	248	27	60	27
4 std.	35	72	11	74	2	9	2	20	3077	2	13	3	51	3	40	4	7	4
8 avg.	39	101	17	374	13	86	15	174	1809	14	25	14	60	24	308	24	54	23
8 std.	38	123	12	80	3	13	2	46	2715	2	9	2	13	6	51	4	6	4
11 avg.	102	93	56	458	26	102	18	226	2009	17	39	22	121	28	232	35	73	36
11 std.	147	47	51	46	14	5	1	30	1097	1	4	1	58	7	39	4	10	3
SS avg.	47	124	33	453	15	98	15	201	6403	17	33	17	119	24	268	27	59	27
SS std.	52	93	21	100	5	15	2	39	5246	3	13	6	61	6	52	5	9	5
OESa nodes																		
2 avg.	34	240	139	458	37	139	26	274	193	30	14	47	131	88	359	47	98	46
2 std.	6	22	179	158	2	26	0	44	198	8	4	38	10	9	85	6	2	1
7 avg.	43	626	19	405	16	101	20	241	130	21	17	20	83	36	231	N.M.	N.M.	N.M.
7 std.	13	208	23	114	2	18	1	42	158	3	5	4	11	3	25	N.M.	N.M.	N.M.
9 avg.	42	353	21	533	17	101	21	261	257	18	21	19	81	33	252	34	76	37
9 std.	18	197	25	152	3	7	3	19	371	3	12	3	8	11	44	4	12	6
OESa avg.	40	396	55	500	19	105	22	263	222	21	19	23	89	40	267	36	79	38
OESa std.	17	217	112	145	7	16	5	33	314	5	10	13	20	19	65	6	13	7
OESb nodes																		
1 avg.	141	845	304	810	20	59	13	142	125	11	18	14	56	19	221	25	44	19
1 std.	74	417	169	648	7	14	2	30	24	2	3	1	5	3	14	0	0	0
10 avg.	209	427	57	1046	14	76	14	192	143	13	27	15	58	26	260	25	57	28
10 std.	82	106	40	188	3	6	1	13	82	2	4	4	2	5	34	2	9	5
OESb avg.	170	666	198	911	18	66	14	163	133	12	22	14	57	22	238	25	52	25
OESb std.	79	375	180	487	6	14	2	35	51	2	6	3	4	5	30	2	10	6
NSa nodes																		
3 avg.	42	151	27	511	7	73	12	135	251	5	13	13	25	33	598	36	77	39
3 std.	11	125	22	227	2	16	1	14	232	0	11	1	12	5	157	4	5	3
5 avg.	101	371	49	3822	8	68	17	238	541	11	18	16	45	39	292	43	93	47
5 std.	76	8	42	655	2	11	1	8	676	1	6	2	8	4	8	2	1	1
12 avg.	66	249	30	860	9	60	14	189	147	10	16	16	65	43	296	42	96	47
12 std.	30	47	18	189	3	20	4	29	96	2	1	3	22	6	53	9	24	11
NSa avg.	63	233	33	1363	8	67	14	176	281	8	15	15	42	37	429	39	87	43
NSa std.	40	121	24	1432	2	16	3	47	322	3	7	2	23	7	189	6	15	7
NSb nodes																		
6 avg.	14	59	30	900	6	179	11	252	91	8	23	12	53	23	243	22	41	20
6 std.	6	11	32	57	0	115	7	73	105	5	1	9	49	0	23	6	18	6

Abbreviations: SS: Shaft Schist Formation; OES: Ore Equivalent Schist; NS: Namies Schist Formation. N.M.: not measured. Note: Averages and standard deviation have been calculated using the values of Appendix B. "Misclassified" samples are not included in the calculations.

certainty (Table 1; Appendices A and B). Therefore, their major and trace element geochemistry is highly coincident with that of their corresponding stratigraphic units, and it is highly likely that their stratigraphic classification is correct.

The Namiesberg stratigraphic succession is similar to that encountered at Gamsberg, with gneiss overlain by psammo-pelitic schists and orthoquartzites (Lipson, 1990). Based on textural appearance, associated lithologies and mineralogical composition, the schists located between the basal gneiss and the white orthoquartzite at Namiesberg were correlated with the NS (Moore, 1977; Lipson, 1990; C.R. McClung, unpublished data). However, examination of the geochemical data distribution reveals that for both the log-normalized major and trace element datasets, a large proportion of the "misclassified" data (80% and 54%, respectively; Appendices A and B), corresponds to the samples from Namiesberg. For both databases the GCS map associated all the Namiesberg SS samples to OES, and all the Namiesberg NS samples to SS (Appendices A and B). Therefore, the geochemical composition of the Namiesberg SS samples resembles the average OES composition, and the geochemical composition of the Namiesberg NS

Table 6
Average modal mineralogy vs. average major element geochemistry of the studied schist units

Node	QZ	SiO_2	Al_2O_3	TiO_2	K_2O
Abundance of quartz in descending order:					
9	65	72.22	11.22	0.48	2.12
2	55	72.43	11.15	0.44	3.25
12	55	81.95	8.77	0.41	2.29
3	53	83.76	7.93	0.32	2.55
5	49	69.64	14.98	0.65	3.89
4	45	69.20	16.21	0.68	3.08
10	38	61.53	19.39	0.95	4.78
6	36	62.41	19.01	0.74	4.39
8	35	62.43	19.13	0.81	4.08
1	0	40.30	26.56	1.35	3.79
Str. unit	QZ	SiO_2	Al_2O_3	TiO_2	K_2O
NSb	54	82.67	8.43	0.37	2.39
NSa	51	70.68	13.55	0.57	3.65
SS	38	65.69	17.66	0.71	3.75
OESa	30	59.51	20.09	0.92	4.29

Concentration of K_2O in descending order:

Node	K_2O	QZ	BI	MS	MS+Sr
10	4.78	38	23	3	13
6	4.39	36	23	8	23
8	4.08	35	17	13	18
5	3.89	49	13	23	27
1	3.79	0	45	10	10
2	3.25	55	13	12	22
4	3.08	45	18	11	26
3	2.55	53	8	5	20
12	2.29	55	10	15	15
9	2.12	65	10	5	5
Str. unit	K_2O	QZ	BI	MS	MS+Sr
OESa	4.29	30	23	9	16
SS	3.75	38	22	9	24
NSa	3.65				0
NSb	2.39	54	9	10	25

Abundance of garnet in descending order:			*Abundance of biotite/chlorite in descending order:*		
Node	GR	MnO	Node	BI+CH	MgO
1	25	0.88	1	45	1.79
8	17	0.34	6	26	1.72
9	13	0.23	10	23	1.83
10	5	0.20	4	23	1.22
3	3	0.22	8	17	1.05
5	2	0.16	2	13	0.26
12		0.07	5	13	0.65
2		0.06	9	10	0.53
4		0.04	12	10	0.45
6		0.04	3	8	0.36

Table 6 (*continued*)

Abundance of garnet in descending order:			*Abundance of biotite/chlorite in descending order:*		
Str. unit	GR	MnO	Str. unit	BI+CH	MgO
OESa	14	0.35	SS	26	1.48
NSb	3	0.13	OESa	23	1.41
NSa	2	0.12	NSb	9	0.41
SS		0.04	NSa	0	0.50

The node numbers correspond to those resulting from the GCS map analysis of the log-normalized major element dataset (Table 3). The average modal values have been calculated from the data of Lipson (1990), whereas the average geochemical concentrations have been extracted from Table 3. Abbreviations: SS: Shaft Schist Formation; OES: Ore Equivalent Schist; NS: Namies Schist Formation; QZ: quartz; BI: biotite or biotite/chlorite; CH: chlorite; GR: garnet; MS: muscovite; Sr: sericite.

samples resembles the average SS composition. These geochemical biases may have been the result of two possibilities, either (a) lithological misclassification of the Namiesberg schists, or (b) in contrast, the apparent misclassification of the Namiesberg NS samples may indicate the presence of a new prospective unit which may not have been evaluated previously, a result that may have obvious implications for exploration in the area.

For both datasets, the GCS maps result from the analysis of both major and trace element datasets (Figs. 3 and 4) with the SS cluster constitutes a coherent group with no apparent subdivisions. This is coincident with the description of its lithology as relatively homogeneous unit (Lipson, 1990). In contrast, two different OES (OESa and OESb) and NS (NSa and NSb) subclusters were distinguished in terms of both major and trace elements. The GCS algorithm projection from a high-dimensional space onto a 2-dimensional space with preservation of the input space topology (e.g. neighbor input vectors are mapped together in the 2-dimensional space) is not free. It is, therefore, not always possible after this strong dimension reduction that neighbor vectors in a high-dimensional space are also neighbors after the mapping in the 2-dimensional space. For this reason, a given cluster in the high-dimensional input space may sometimes be divided in two after projection. In all cases the algorithm tries to preserve the space topology as much as possible. However, close examination reveals consistency in the OES and NS data distribution, with almost equivalent sample groupings defining the OES and NS subclusters, for both the major and trace element dataset (Appendices A and B). Therefore, it is highly likely that the OES and NS subdivisions are related with true lithological variations within these stratigraphic units.

6.3. Geochemical, mineralogical and lithological relations

As for the major and trace element geochemistry, there are relevant differences in the modal mineralogical content between the different stratigraphic-related units. The geochemical and mineralogical relations of Table 6 show that the concentration of some of the major elements are directly correlated with the abundance of particular framework minerals as quartz (correlated with SiO_2), biotite (correlated with K_2O and MgO), chlorite (correlated with MgO) and garnet (correlated with MnO). Table 6 also shows the inverse relationship between the modal content of quartz and the concentrations of Al_2O_3 and TiO_2, reflecting the dilution of the clay mineral fraction of the studied schists by detrital quartz.

The high to very high S content of the SS, along with the relatively low Pb, Zn and Cu concentrations of this unit (Table 4) could indicate the presence of iron-sulfide minerals, probably in the form of pyrite. This is in good agreement with the pyritic banding that characterizes the lowermost parts of SS and that have been interpreted as a reducing environment of deposition (Lipson, 1990).

OESa represents pelitic schists (low SiO_2, high Al_2O_3 and associated TiO_2, Table 2) lateral to the ore bodies, whereas OESb tends toward more psammitic schists. OESb represents a unit more closely related to the mineralization due to its higher base metal content. Accordingly, the high Zn and Pb concentrations associated with OESb (Table 4) are to be expected since base metal sulfides, including galena, sphalerite and chalcopyrite, are disseminated throughout (Ryan et al., 1986). OESb also contains very high Ba concentrations that are likely to be indicative of proximity to a hydrothermal source (Table 4).

In contrast to SS, the low pyrite and pyrrhotite content of the NS, constituting only 5% of the rock mass along with accessory chalcopyrite (Lipson, 1990), can account for the observed low S content of some NS samples (Table 4). The pattern of high P_2O_5, Zr, La, Ce and Nd in NSa (Tables 2 and 4) is compatible with the concentration of zircon and REE-phosphates, the later being probably apatite, a common accessory mineral in all the studied schist units (Ryan et al., 1986; Lipson, 1990; Stalder and Rozendaal, 2005). The concentration of these minerals suggests a recycled provenance from a first-cycle felsic source, which is also compatible with the low to very low average Sr concentration of NSa (Table 4; Lacassie et al., 2004). Similarly, the very high SiO_2, coupled with the low Al_2O_3, CaO, Na_2O, FeOt, TiO_2, Co, Ni, Sc and V concentrations that are associated with NSb (Tables 2 and 4), are geochemical features of sandstones of a recycled provenance from a felsic source (Lacassie et al., 2004). Thus, part of the geochemical differences between both NS units (NSa and NSb) could be only a reflection of the grain size difference between them, with NSb having a more "sandy" character (Fig. 2). However, the high average concentration of Ba that is associated with NSa is likely to be a hydrothermal overprint of a low-temperature, Ba-enriched fluid. This is supported by the known barite occurrences in the study area. The NSa subregion of the trace element dataset defined by three samples from Broken Hill (node 5; Appendix B), and is characterized by a very high average concentration of Ba and anomalously high average concentrations of Pb, Zn and Cu, which are comparable to the average Pb, Zn and Cu concentrations of OESa (Table 4). This seems to contradict the barren/unmineralized character of NS and suggests that a portion of this unit was altered by hydrothermal fluids moving through it. The last interpretation is supported by the shift to lower $\delta^{18}O$ values in the NS compared to the other units (Lipson, 1990). Therefore, NS may either be a new prospective unit, or the elevated base-metal content could be a result of the close-spatial association of the NS with a major ore deposit. These relations also emphasize the character of Ba as an element that may point to mineralization.

7. Conclusions

Self-organizing neural maps (GCS maps in our case) provide useful information on geochemical differences between different schists units of the Bushmanland Group (SS, OES and NS) in the study area. They highlight higher order correlations and allow visual perception of subtle inter-relations between variables. The GCS map reveals important differences within stratigraphic units that have not been previously recognized.

The major and trace element geochemistry of the samples from Plant Hill, Tank Hill, Maanhaarkop and Wortel, is highly coincident with that of their corresponding stratigraphic units, and suggests it is highly likely that their original stratigraphic classification was correct (see Lipson, 1990). However, the geochemical signature of the NS and SS samples from Namiesberg resemble SS and OES from all other localities. This suggests either (a) that the NS and SS units at Namiesberg have been misidentified during their original mapping and that the lithostratigraphy of the Namiesberg structural succession has been misunderstood, or (b) that a new prospective unit occurs at Namiesberg that warrants further exploration. Either option indicates that the Namiesberg area is a highly prospective terrane that has not received sufficient attention during previous exploration efforts.

The ANN approach has also identified sub-divisions of certain units, such as the Namies Schist (NSa and NSb) and

the Ore Equivalent Schist (OESa and OESb). Fundamental differences between OESa and OESb indicate that the latter is more closely associated with base metal mineralization than the former, whereas NSa has a larger pelitic component compared to NSb that is more psammitic and transitional into the overlying quartzite units. These subdivisions within the ANN analyses highlights the geochemical features that have both useful geological and petrographic discriminators, as well as exploration potential as pointers to nearby mineralization.

The results of this study indicate that ANN analyses of large high-dimensional geochemical datasets could be an important tool for regional mineral exploration, as well as for the prediction of mineral prospectivity. It could be a particularly useful exploratory tool within highly deformed and metamorphosed terrains, such as the metasedimentary Bushmanland Group, where isolated outcrop, as well as the complex deformational and metamorphic history of the area hampers regional correlation and the identification of stratigraphic units by means of fieldwork and petrography alone.

Finally, it is important to note that the addition of more data, either by increasing the sampling density from localities already examined or by including other localities to the analysis will almost certainly increase the separation between the groups, as the characteristic elemental fingerprints observed in each stratigraphic unit become more accurately defined. This, in turn, will increase the reliability of assigning samples of uncertain stratigraphic position to specific schist units, and consequently serve as important pointer towards prospective areas.

Acknowledgements

We are grateful to Professor Nic Beukes (University of Johannesburg) for his support during the preparation of this manuscript. This work was conducted by using the Growing Cell Structure Visualisation (GCSVIS) Toolbox, written and developed by Andrew J. Walker, Dr. Robert F. Harrison and Dr. Simon S. Cross in the Departments of Automatic Control and Systems Engineering and Pathology at the University of Sheffield, United Kingdom.

Appendix A

Major element data for samples of the stratigraphic-related units resulting from the ANN analysis of the log-normalized major elements dataset (Fig. 3)

Node	Sample	Location	Unit	SiO_2	Al_2O_3	FeOt	MnO	MgO	CaO	Na_2O	K_2O	TiO_2	P_2O_5
SS nodes													
4	ALP060	Broken Hill	SS	66.73	17.44	5.37	0.03	1.47	0.11	0.35	3.56	0.72	0.02
4	ALP158	Broken Hill	SS	68.90	16.29	4.82	0.03	1.14	0.15	0.19	2.98	0.65	0.04
4	ALP160	Broken Hill	SS	70.84	15.59	4.48	0.02	0.97	0.12	0.19	2.90	0.63	0.03
4	ALP161	Broken Hill	SS	67.87	16.70	4.96	0.03	1.26	0.15	0.31	2.97	0.72	0.04
4	ALP162	Broken Hill	SS	69.20	16.15	4.62	0.03	1.11	0.14	0.33	2.66	0.67	0.05
4	ALP185	Broken Hill	SS	65.63	18.21	4.87	0.03	1.49	0.16	0.32	3.75	0.73	0.03
4	ALP136	Plant Hill	SS	70.17	16.19	4.66	0.04	1.10	0.10	0.16	2.94	0.66	0.04
4	ALP137	Plant Hill	SS	68.73	16.73	4.92	0.09	1.21	0.10	0.15	3.02	0.70	0.03
4	ALP138	Plant Hill	SS	69.35	16.00	4.66	0.03	1.24	0.09	0.19	3.21	0.72	0.03
4	ALP139	Plant Hill	SS	69.49	15.73	4.35	0.03	1.24	0.15	0.31	2.83	0.68	0.02
4	ALP140	Plant Hill	SS	72.19	14.41	4.18	0.03	1.02	0.11	0.20	2.86	0.58	0.05
4	ALP141	Plant Hill	SS	71.76	14.74	4.72	0.03	1.00	0.09	0.17	2.91	0.63	0.02
4	ALP142	Plant Hill	SS	70.71	15.45	4.74	0.03	1.13	0.11	0.23	2.90	0.65	0.03
4	ALP442	Wortel	STS	67.23	17.31	5.88	0.05	1.66	0.07	0.19	3.57	0.71	0.04
6	ALP056	Broken Hill	SS	60.40	19.52	5.89	0.07	1.93	0.17	0.28	4.66	0.82	0.06
6	ALP057	Broken Hill	SS	61.28	18.90	6.01	0.05	1.69	0.19	0.35	4.72	0.74	0.07
6	ALP058	Broken Hill	SS	61.18	19.42	6.24	0.04	1.67	0.14	0.24	4.59	0.71	0.08
6	ALP059	Broken Hill	SS	61.91	18.95	5.99	0.03	1.72	0.12	0.24	4.19	0.74	0.05
6	ALP087	Broken Hill	SS	62.53	19.28	5.64	0.03	1.86	0.16	0.14	4.50	0.72	0.06
6	ALP087A	Broken Hill	SS	61.51	19.03	6.13	0.04	1.74	0.18	0.18	4.46	0.75	0.06
6	ALP087F	Broken Hill	SS	59.65	18.79	7.27	0.04	1.65	0.14	0.23	4.77	0.77	0.04
6	ALP154	Broken Hill	SS	64.24	18.29	5.02	0.03	1.58	0.16	0.30	4.40	0.68	0.05
6	ALP154A	Broken Hill	SS	61.21	19.50	5.56	0.04	1.85	0.16	0.17	4.47	0.74	0.04
6	ALP155	Broken Hill	SS	64.21	18.84	4.97	0.03	1.60	0.15	0.28	3.79	0.78	0.04
6	ALP156	Broken Hill	SS	64.46	18.17	5.57	0.04	1.75	0.19	0.40	3.81	0.78	0.03
6	ALP183	Broken Hill	SS	62.05	19.80	4.68	0.03	1.82	0.07	0.20	4.64	0.74	0.06
6	ALP184	Broken Hill	SS	62.33	19.39	5.27	0.03	1.75	0.08	0.25	4.45	0.71	0.05
6	ALP186	Broken Hill	SS	65.38	17.90	4.95	0.03	1.49	0.19	0.35	3.68	0.77	0.04
6	ALP157	Broken Hill	SS	62.75	18.93	5.36	0.02	1.47	0.25	0.49	4.35	0.64	0.07
6	ALP440	Wortel	STS	63.79	19.32	5.88	0.07	1.74	0.16	0.29	4.66	0.72	0.06

Appendix A (*continued*)

Node	Sample	Location	Unit	SiO_2	Al_2O_3	FeOt	MnO	MgO	CaO	Na_2O	K_2O	TiO_2	P_2O_5
OESa nodes													
1	***ALP422**	**Namiesberg**	**STS**	**47.47**	**29.12**	**9.05**	**0.22**	**2.42**	**0.10**	**0.10**	**5.05**	**1.13**	**0.08**
1	ALP212	Broken Hill	OES	44.55	24.46	16.53	0.89	1.32	0.35	0.13	3.41	1.03	0.05
1	ALP037	Maanhaarkop	OES	36.04	28.65	19.99	0.87	2.26	0.67	0.16	4.17	1.66	0.03
8	***ALP430**	**Namiesberg**	**STS**	**57.13**	**22.40**	**7.82**	**0.12**	**1.68**	**0.10**	**0.12**	**4.60**	**0.90**	**0.06**
8	***ALP431**	**Namiesberg**	**STS**	**59.05**	**21.34**	**7.14**	**0.19**	**1.87**	**0.12**	**0.10**	**4.13**	**0.86**	**0.07**
8	ALP171	Broken Hill	OES	67.73	18.84	5.69	0.23	1.26	0.14	0.09	4.43	0.81	0.08
8	ALP172	Broken Hill	OES	61.49	19.68	7.64	0.25	1.41	0.13	0.07	4.03	0.90	0.05
8	ALP173	Broken Hill	OES	62.75	18.58	8.54	0.36	1.11	0.12	0.06	3.23	0.84	0.03
8	ALP175	Broken Hill	OES	63.68	18.12	7.54	0.30	0.94	0.12	0.06	3.86	0.81	0.06
8	ALP176	Broken Hill	OES	60.19	20.04	7.80	0.48	0.92	0.14	0.06	4.62	0.86	0.04
8	ALP191	Broken Hill	OES	63.68	16.86	8.29	0.31	1.22	0.14	0.07	2.55	0.72	0.04
8	ALP206	Broken Hill	OES	63.83	18.03	5.81	0.45	1.00	0.13	0.09	3.70	0.75	0.04
8	ALP207	Broken Hill	OES	59.94	21.01	6.22	0.37	0.66	0.09	0.12	5.47	0.81	0.07
8	ALP208	Broken Hill	OES	58.59	20.99	8.11	0.31	0.93	0.15	0.12	4.84	0.81	0.04
10	***ALP054**	**Broken Hill**	**SS**	**61.63**	**19.79**	**7.59**	**0.40**	**0.97**	**0.29**	**0.20**	**4.42**	**0.79**	**0.04**
10	***ALP424**	**Namiesberg**	**STS**	**55.92**	**22.28**	**7.05**	**0.11**	**2.48**	**0.13**	**0.11**	**5.18**	**0.99**	**0.08**
10	ALP189	Broken Hill	OES	64.40	17.65	5.75	0.17	1.90	0.18	0.35	4.93	0.79	0.08
10	ALP190	Broken Hill	OES	59.04	22.35	6.21	0.12	1.76	0.12	0.13	4.97	0.99	0.05
10	ALP210	Broken Hill	OES	60.72	18.33	8.74	0.48	1.74	0.26	0.27	3.99	0.74	0.06
10	ALP014	Maanhaarkop	OES	63.38	17.76	6.48	0.14	1.98	0.19	0.23	4.46	0.84	0.06
10	ALP034	Maanhaarkop	OES	60.22	20.51	6.16	0.13	2.02	0.25	0.28	5.14	0.88	0.08
10	ALP035	Maanhaarkop	OES	61.41	19.71	5.73	0.14	1.59	0.19	0.35	5.21	1.48	0.05
OESb nodes													
7	ALP203	Broken Hill	OES	73.70	11.02	6.88	0.64	0.74	0.11	0.07	1.96	0.45	0.02
7	ALP225	Maanhaarkop	OES	74.94	10.66	6.47	0.09	1.10	0.17	0.14	2.42	0.47	0.03
9	ALP194	Broken Hill	OES	72.27	11.43	8.00	0.03	0.42	0.07	0.12	1.93	0.52	0.07
9	ALP198	Broken Hill	OES	74.88	9.54	8.90	0.32	0.29	0.06	0.10	1.63	0.38	0.08
9	ALP199	Broken Hill	OES	71.76	12.31	6.74	0.25	0.47	0.06	0.09	2.61	0.59	0.08
9	ALP202	Broken Hill	OES	71.39	10.28	10.47	0.29	0.40	0.09	0.07	2.18	0.38	0.08
9	ALP219	Maanhaarkop	OES	70.79	12.54	8.51	0.28	1.05	0.36	0.08	2.26	0.54	0.17
11	ALP192	Broken Hill	OES	67.26	14.46	7.94	0.03	0.46	0.04	0.16	2.59	0.60	0.06
11	ALP200	Broken Hill	OES	70.73	13.22	6.99	0.17	0.54	0.06	0.13	3.15	0.55	0.05
11	ALP201	Broken Hill	OES	69.64	14.94	5.98	0.51	0.60	0.03	0.07	3.19	0.63	0.04
11	ALP209	Broken Hill	OES	65.61	17.47	5.79	0.08	0.38	0.06	0.19	5.03	0.63	0.06
11	ALP131	Maanhaarkop	OES	70.04	15.83	6.31	0.04	1.14	0.04	0.08	3.09	0.87	0.03
11	ALP217	Maanhaarkop	OES	69.96	14.47	5.52	0.13	0.83	0.08	0.09	3.01	0.66	0.08
11	ALP221	Maanhaarkop	OES	66.97	16.40	6.42	0.10	0.73	0.06	0.09	3.10	0.65	0.06
NSa nodes													
2	ALP244	Tank Hill	NTS	69.99	12.93	5.61	0.07	0.39	0.02	0.18	3.62	0.66	0.16
2	ALP205	Broken Hill	NS	72.25	11.12	9.20	0.10	0.20	0.09	0.21	3.28	0.36	0.16
2	ALP236	Maanhaarkop	NS	75.05	9.40	8.94	0.01	0.20	0.12	0.30	2.85	0.31	0.15
5	ALP030	Broken Hill	NS	71.45	13.35	7.18	0.17	0.58	0.16	0.08	3.66	0.58	0.10
5	ALP061	Broken Hill	NS	67.17	16.32	6.79	0.22	0.86	0.17	0.15	3.48	0.64	0.07
5	ALP062	Broken Hill	NS	69.51	15.43	5.35	0.11	0.66	0.12	0.14	4.38	0.62	0.07
5	ALP063	Broken Hill	NS	69.78	15.23	5.49	0.12	0.37	0.11	0.11	4.53	0.62	0.04
5	ALP122	Maanhaarkop	NS	70.27	14.59	7.47	0.18	0.76	0.15	0.22	3.40	0.80	0.08
NSb nodes													
3	ALP243	Broken Hill	NS	82.83	7.20	4.38	0.27	0.31	0.17	0.14	2.62	0.21	0.04
3	ALP123	Maanhaarkop	NS	84.69	8.65	2.65	0.16	0.40	0.16	0.25	2.48	0.42	0.02
12	ALP039	Broken Hill	NS	82.03	9.34	3.69	0.09	0.36	0.04	0.07	2.36	0.47	0.04
12	ALP064	Broken Hill	NS	80.20	8.62	5.89	0.10	0.52	0.09	0.07	2.05	0.35	0.06
12	ALP065	Broken Hill	NS	83.62	8.35	3.01	0.03	0.46	0.03	0.09	2.46	0.40	0.03

Abbreviations: SS: Shaft Schist; OES: Ore Equivalent Schist; NS: Namies Schist. *"Misclassified" samples (in bold letters). To distinguish between the rocks from Broken Hill and their regional counterparts (outside of the immediate Aggeneys area), the suffix "type" (T) is added to the Broken Hill name for the corresponding regional rock (i.e. Shaft-type Schist (STS) or Namies-type Schist (NTS)).

Appendix B

Trace element data for the stratigraphic-related units resulting from the ANN analysis of the trace element dataset (Fig. 4)

Node	Sample	Location	Unit	Pb	Zn	Cu	Ba	Co	Cr	Ni	Rb	S	Sc	Sr	Th	V	Y	Zr	La	Ce	Nd
SS nodes																					
4	ALP056	Broken Hill	SS	94	223	57	622	15	125	19	230	12,141	22	61	24	227	23	258	28	63	29
4	ALP057	Broken Hill	SS	88	198	52	644	16	109	17	222	14,256	19	63	18	258	20	226	27	58	27
4	ALP058	Broken Hill	SS	42	152	48	549	17	103	15	233	14,094	19	45	17	183	22	218	22	50	23
4	ALP059	Broken Hill	SS	31	144	52	543	16	108	14	218	11,830	19	47	16	180	22	240	25	58	26
4	ALP060	Broken Hill	SS	31	114	28	450	16	100	13	183	10,422	19	48	21	106	25	285	29	66	30
4	ALP087	Broken Hill	SS	49	160	46	601	14	131	14	227	11,542	18	29	17	196	22	212	N.M.	N.M.	N.M.
4	ALP087A	Broken Hill	SS	38	135	34	527	13	102	16	206	14,198	20	25	20	139	23	223	N.M.	N.M.	N.M.
4	ALP087F	Broken Hill	SS	51	125	46	526	19	103	14	210	18,501	20	23	18	125	20	224	N.M.	N.M.	N.M.
4	ALP154	Broken Hill	SS	30	144	26	538	13	100	14	240	7611	19	32	18	145	27	228	N.M.	N.M.	N.M.
4	ALP154A	Broken Hill	SS	22	195	44	545	16	113	16	241	8556	22	27	20	192	28	238	N.M.	N.M.	N.M.
4	ALP155	Broken Hill	SS	109	119	25	453	13	105	17	217	8198	18	38	16	107	27	286	30	64	30
4	ALP156	Broken Hill	SS	16	114	32	474	14	110	17	232	9293	19	41	19	113	23	279	33	73	31
4	***ALP157**	**Broken Hill**	**OES**	**128**	**112**	**44**	**559**	**16**	**94**	**13**	**231**	**11,837**	**17**	**49**	**15**	**153**	**26**	**180**	**36**	**67**	**32**
4	ALP161	Broken Hill	SS	8	60	27	405	14	99	16	172	7053	17	40	12	99	16	317	20	48	20
4	ALP183	Broken Hill	SS	36	391	52	561	22	116	15	242	7286	19	22	18	244	26	212	25	53	24
4	ALP184	Broken Hill	SS	23	128	50	526	15	109	14	235	8395	19	22	14	202	19	211	27	60	26
4	ALP185	Broken Hill	SS	23	102	31	408	13	100	15	198	7608	16	37	17	112	24	268	31	67	31
4	ALP186	Broken Hill	SS	21	100	31	452	12	107	17	204	8650	18	49	17	114	22	280	26	57	26
4	ALP138	Plant Hill	SS	5	72	37	378	13	100	16	201	9416	17	22	13	115	18	328	24	56	23
8	ALP158	Broken Hill	SS	10	69	18	351	12	97	14	167	4339	15	31	17	92	21	307	23	52	23
8	ALP160	Broken Hill	SS	6	35	2	287	11	89	15	174	129	15	28	15	51	17	337	20	50	19
8	ALP162	Broken Hill	SS	60	67	23	385	12	89	15	162	8276	15	44	18	72	24	325	24	63	27
8	ALP136	Plant Hill	SS	18	75	44	276	13	93	14	199	1256	15	15	14	52	20	347	24	51	21
8	ALP137	Plant Hill	SS	120	78	11	294	11	96	15	205	675	16	17	16	57	18	334	23	55	22
8	ALP139	Plant Hill	SS	12	65	21	416	11	92	14	175	6344	15	40	16	75	18	345	25	54	19
8	ALP140	Plant Hill	SS	70	54	10	304	10	84	13	197	797	14	23	14	46	19	341	20	49	21
8	ALP141	Plant Hill	SS	7	64	7	327	13	94	17	206	531	15	23	13	50	26	350	23	58	24
8	ALP142	Plant Hill	SS	8	56	6	360	11	95	15	203	599	15	29	14	52	23	355	23	57	24
8	ALP217	Maanhaarkop	SS	64	91	16	408	13	79	17	196	102	15	19	14	61	32	251	28	60	29
8	ALP221	Maanhaarkop	SS	33	64	5	480	14	85	16	184	63	14	22	13	66	34	209	32	59	28
8	***ALP203**	**Broken Hill**	**OES**	**91**	**509**	**36**	**433**	**13**	**66**	**12**	**29**	**224**	**12**	**12**	**11**	**52**	**29**	**277**	**24**	**56**	**28**
8	***ALP225**	**Maanhaarkop**	**OES**	**14**	**87**	**22**	**541**	**22**	**53**	**12**	**167**	**181**	**10**	**19**	**9**	**53**	**33**	**225**	**18**	**40**	**20**
8	***ALP401**	**Namiesberg**	**NTS**	**14**	**80**	**39**	**486**	**12**	**92**	**14**	**195**	**237**	**15**	**23**	**15**	**61**	**25**	**338**	**30**	**63**	**30**
8	***ALP411**	**Namiesberg**	**NTS**	**5**	**72**	**29**	**445**	**7**	**79**	**13**	**147**	**146**	**12**	**13**	**18**	**43**	**24**	**376**	**26**	**57**	**25**
8	***ALP415**	**Namiesberg**	**NTS**	**21**	**60**	**49**	**799**	**9**	**100**	**15**	**221**	**187**	**16**	**23**	**16**	**76**	**18**	**297**	**26**	**57**	**25**
11	ALP054	Broken Hill	SS	272	141	28	461	41	99	19	217	788	17	43	21	73	36	227	39	87	41
11	ALP440	Wortel	STS	24	91	114	503	21	107	18	259	2330	18	39	22	185	24	196	37	73	35
11	ALP442	Wortel	STS	10	48	25	411	15	99	18	202	2910	16	35	22	104	25	273	36	66	33
11	***ALP219**	**Maanhaarkop**	**OES**	**16**	**89**	**25**	**312**	**23**	**68**	**14**	**160**	**92**	**12**	**13**	**45**	**121**	**44**	**235**	**29**	**66**	**36**
OESa nodes																					
2	***ALP422**	**Namiesberg**	**STS**	**16**	**312**	**445**	**573**	**23**	**109**	**40**	**342**	**3995**	**27**	**9**	**33**	**130**	**40**	**410**	**70**	**133**	**68**
2	ALP212	Broken Hill	OES	38	255	265	570	38	120	26	243	333	24	16	74	138	81	419	51	99	47
2	ALP037	Maanhaarkop	OES	30	224	12	346	35	157	26	305	53	35	11	20	124	94	299	43	96	45
7	ALP176	Broken Hill	OES	40	569	4	444	14	103	19	264	366	20	11	22	88	40	215	N.M.	N.M.	N.M.
7	ALP190	Broken Hill	OES	52	557	6	499	18	126	22	286	35	25	21	25	94	33	267	N.M.	N.M.	N.M.
7	ALP191	Broken Hill	OES	26	928	52	239	15	84	19	191	49	22	14	17	70	37	214	N.M.	N.M.	N.M.
7	ALP206	Broken Hill	OES	54	450	13	436	17	91	20	224	68	18	21	17	78	34	228	N.M.	N.M.	N.M.
9	***ALP430**	**Namiesberg**	**STS**	**8**	**151**	**38**	**730**	**23**	**81**	**22**	**244**	**204**	**23**	**19**	**23**	**108**	**43**	**249**	**44**	**88**	**45**
9	***ALP431**	**Namiesberg**	**STS**	**32**	**208**	**57**	**636**	**20**	**74**	**22**	**234**	**631**	**19**	**28**	**27**	**97**	**50**	**282**	**57**	**110**	**55**
9	ALP171	Broken Hill	OES	47	397	17	547	14	93	21	256	208	16	13	18	73	30	249	33	75	36
9	ALP172	Broken Hill	OES	50	483	14	490	17	107	25	256	336	17	8	17	83	29	264	29	71	35
9	ALP173	Broken Hill	OES	30	535	89	401	18	96	26	235	1056	21	7	24	80	35	264	38	80	37
9	ALP175	Broken Hill	OES	28	563	48	432	15	101	19	236	1003	18	8	19	79	36	298	28	69	35
9	ALP189	Broken Hill	OES	35	431	4	788	17	96	18	269	40	18	30	18	67	33	277	35	76	37
9	ALP207	Broken Hill	OES	86	671	6	634	13	99	19	280	77	19	28	15	86	29	183	31	72	34
9	ALP208	Broken Hill	OES	39	411	15	613	14	104	19	266	59	19	27	23	96	28	189	37	76	38
9	ALP210	Broken Hill	OES	47	214	10	513	19	87	19	261	49	18	13	17	73	54	207	30	57	27

Appendix B (*continued*)

Node	Sample	Location	Unit	Pb	Zn	Cu	Ba	Co	Cr	Ni	Rb	S	Sc	Sr	Th	V	Y	Zr	La	Ce	Nd
OESa nodes																					
9	ALP014	Maanhaarkop	OES	22	107	21	414	17	103	21	262	82	20	25	16	82	39	287	33	70	33
9	ALP034	Maanhaarkop	OES	60	121	5	654	18	111	20	291	53	21	34	19	88	30	215	34	70	33
9	ALP035	Maanhaarkop	OES	44	108	27	684	14	100	20	287	69	23	43	24	79	47	266	42	98	51
9	ALP131	Maanhaarkop	OES	19	193	0	231	26	111	25	236	57	10	15	22	83	11	319	40	97	45
9	***ALP122**	**Maanhaarkop**	**NS**	**18**	**99**	**87**	**414**	**16**	**132**	**19**	**223**	**263**	**14**	**21**	**14**	**53**	**29**	**486**	**42**	**92**	**47**
OESb nodes																					
1	ALP192	Broken Hill	OES	125	1336	250	314	16	75	16	184	106	13	21	15	60	15	230	25	44	19
1	ALP194	Broken Hill	OES	46	497	518	288	14	66	13	131	107	13	15	12	60	20	200	N.M.	N.M.	N.M.
1	ALP198	Broken Hill	OES	176	501	113	985	21	46	11	113	156	9	16	13	50	20	225	N.M.	N.M.	N.M.
1	ALP202	Broken Hill	OES	217	1046	335	1653	29	48	12	139	132	10	20	14	53	22	230	N.M.	N.M.	N.M.
10	ALP199	Broken Hill	OES	293	534	102	1071	17	72	15	187	77	10	23	10	56	20	231	23	50	24
10	ALP200	Broken Hill	OES	129	424	45	1220	12	72	14	206	234	14	31	17	57	28	297	N.M.	N.M.	N.M.
10	ALP201	Broken Hill	OES	204	323	24	847	14	83	14	182	117	14	26	17	60	29	253	26	63	31
NSa nodes																					
3	ALP039	Broken Hill	NS	52	89	54	273	10	83	14	133	589	6	6	14	22	39	779	40	83	42
3	ALP064	Broken Hill	NS	34	328	2	766	8	60	11	116	71	5	8	12	42	33	451	38	78	39
3	ALP065	Broken Hill	NS	51	144	17	630	7	90	12	138	140	6	9	13	19	30	483	34	75	38
3	ALP123	Maanhaarkop	NS	30	44	35	374	4	57	11	151	205	5	29	13	16	28	678	32	70	35
5	ALP062	Broken Hill	NS	47	365	19	3358	9	60	16	232	63	10	22	17	50	42	286	44	92	48
5	ALP063	Broken Hill	NS	154	376	78	4285	6	75	18	244	1019	12	14	14	39	36	297	41	93	46
5	***ALP209**	**Broken Hill**	**OES**	**51**	**483**	**44**	**2601**	**6**	**69**	**16**	**259**	**36**	**16**	**28**	**11**	**72**	**21**	**238**	**31**	**67**	**29**
12	ALP030	Broken Hill	NS	58	260	49	769	10	74	15	201	203	10	15	19	65	44	356	44	105	51
12	ALP061	Broken Hill	NS	41	198	29	734	12	38	17	211	201	13	17	14	43	36	257	32	69	35
12	ALP205	Broken Hill	NS	99	290	13	1077	5	69	10	156	36	8	17	15	86	48	275	49	114	55
12	ALP236	Maanhaarkop	NS	0	16	0	402	9	66	10	181	141	7	13	11	71	32	245	37	89	45
NSb nodes																					
6	ALP410	Namiesberg	NTS	10	66	53	940	6	98	16	303	165	11	23	18	87	23	259	26	53	24
6	ALP243	Broken Hill	NS	18	51	8	859	6	260	7	200	16	5	22	5	18	23	227	17	28	15

Abbreviations: SS: Shaft Schist; OES: Ore Equivalent Schist; NS: Namies Schist. *"Misclassified" samples (in bold letters). To distinguish between the rocks from Broken Hill and their regional counterparts (outside of the intermediate Aggeneys area), the suffix "type" (T) is added to the Broken Hill name for the corresponding regional rock (STS and NTS). N.M.: Not measured.

References

Achurra, L., Marquardt, C., Lacassie, J.P., Le Roux, J.P., 2003. Nódulos de Mn de la Formación Bahía Inglesa: Geoquímica, génesis e implicancias paleoambientales. Resúmenes Expandidos, X Congreso Geológico Chileno.

Colliston, W.P., Schoch, A.E., 2002. The structural development of the Aggeneys Hills, Namaqua Metamorphic Complex. South African Journal of Geology 105, 301–324.

De Jager, D.H., 1963. Sillimanite in Namaqualand: review of reserves and report on some low-grade deposits. Bulletin of the Geological Survey of South Africa 40. 42 pp.

De Jager, D.H., von Backström, J.W., 1961. The sillimanite deposits in Namaqualand near Pofadder. Bulletin of the Geological Survey of South Africa 33. 49 pp.

Du Toit, M.C., 1998. Lead. In: Wilson, M.G.C., Anhaeusser, C.R. (Eds.), The mineral resources of South Africa: Pretoria, Council for Geoscience, pp. 424–432.

Fritzke, B., 1994. Growing cell structures—a self-organizing network for unsupervised and supervised learning. Neural Networks 7, 1441–1460.

Hoffmann, D., 1993. Aspects of the geology, geochemistry and metamorphism of the lower orebody, Broken Hill deposit, Aggeneys. Unpublished M.Sc. thesis, University of Cape Town, Cape Town, 211 pp.

Joubert, P., 1974. Geologic map of Aggeneys–Pofadder area: Precambrian Research Unit. Cape Town, University of Cape Town. 1:100,000, 1 sheet.

Joubert, P., 1986. The Namaqualand Metamorphic Complex — a summary. In: Anhaeusser, C.R., Maske, S. (Eds.), Mineral Deposits of Southern Africa, vol. II. Geological Society of South Africa, Johannesburg, pp. 1395–1420.

Lacassie, J.P., Ruiz del Solar, J., Roser, B.P., Belousova, E., Ortiz, E., Hervé, F., 2003a. Discovering geochemical patterns using self-organizing neural networks: a new perspective for analysis in the Earth Sciences. Workshop on Self-Organizing Maps. Hibikino, Japan.

Lacassie, J.P., Roser, B.P., Ruiz del Solar, J., Hervé, F., 2003b. Visualización de patrones geoquímicos mediante Redes Neuronales Artificiales: una nueva perspectiva de análisis para las Ciencias de la Tierra. X Chilean Geol Cong, Abstract.

Lacassie, J.P., Roser, B.P., Ruiz del Solar, J., Hervé, F., 2004. Visualization of geochemical datasets by using neural networks: a novel perspective for sedimentary provenance analysis. Sedimentary Geology 165, 175–191.

Le Maitre, R.W., 1982. Numerical Petrology: Statistical Interpretation of Numerical Data. Elsevier, Amsterdam. 281 pp.

Lipson, R.D., 1990. Lithogeochemistry and origin of metasediments hosting the Broken Hill deposit, Aggeneys, South Africa, and implications for ore genesis: unpublished doctoral thesis, University of Cape Town, Cape Town, 245 pp.

McClung, C.R., Basin analysis of the Bushmanland Group in the Namaqualand Metamorphic Complex, South Africa: unpublished Doctoral thesis, University of Johannesburg, Johannesburg (in preparation).

McLennan, S.M., 1989. Rare earth elements in sedimentary rocks: influence of provenance and sedimentary processes. In: Lipin, B. R., McKay, G.A. (Eds.), Geochemistry and mineralogy of rare earth elements. Reviews in Mineralogy, vol. 21, pp. 169–200.

Moore, J.M., 1977. The geology of the Namiesberg, northern Cape. Bulletin of the Precambrian Research Unit, vol. 20. University of Cape Town, Cape Town. 69 pp.

Moore, J.M., 1989. A comparative study of metamorphosed supracrustal rocks from the western Namaqualand Metamorphic Complex. Bulletin of the Precambrian Research Unit, vol. 37. University of Cape Town, Cape Town. 370 pp.

Novak, D., and Kihn, C., 1994, The base metal deposits of Aggeneys, Northern Cape, unpublished company report, Black Mountain Mine Ltd.

Reid, D.L., Welke, H.J., Smith, C.B., Moore, J.M., 1997. Lead isotope patterns in Proterozoic stratiform mineralization in the Bushmanland Group, Namaqua Province, South Africa. Economic Geology 92, 248–258.

Ryan, P.J., Lawrence, A.L., Lipson, R.D., Moore, J.M., Paterson, A., Stedman, D.P., van Zyl, D., 1986. The Aggeneys base metal sulphide deposits, Namaqualand District. In: Anhaeusser, C.R., Maske, S. (Eds.), Mineral Deposits of Southern Africa: Geological Society of South Africa, Johannesburg, vol. 2, pp. 1447–1474.

Stalder, M., Rozendaal, A., 2005. Apatite nodules as an indicator of depositional environment and ore genesis for the Mesoproterozoic Broken Hill-type Gamsberg Zn–Pb deposit, Namaqua Province, South Africa. Mineralium Deposita 39, 189–203.

Wilson, M.G.C., Anhaeusser, C.R., 1998. The mineral resources of South Africa. Handbook, vol. 16. Council for Geoscience, Pretoria. 740 pp.